Metal-Metal Bonding in Paramagnetic Chromium(III) Complexes – An MO-Theoretical Case Study

Christoph Janiak*[a], Jérôme Silvestre[b], and Klaus H. Theopold[c]

Institut für Anorganische und Analytische Chemie, Technische Universität Berlin[a], Straße des 17. Juni 135, W-1000 Berlin 12, Germany

Rhône-Poulenc Agrochimie[b], 14-20 Rue Pierre-Baizet, 69009 Lyon, France

Department of Chemistry & Biochemistry, University of Delaware[c], Newark, Delaware 19716, USA

Received September 3, 1992

Key Words: Chromium(III) alkyls / Paramagnetism / Calculations, MO / Metal–Metal bonding

The electronic structures of the edge-sharing bioctahedral chromium(III) dimers $\{C_5H_5Cr(CH_3)(\mu\text{-}Cl)\}_2$ (**2**) and $\{Me_5C_5Cr(CH_3)(\mu\text{-}CH_3)\}_2$ (**4***, (Cp* derivative), **4** (Cp derivative)), the trinuclear complex $\{C_5H_5Cr(\mu\text{-}Cl)\}_3(\mu\text{-}CH)$ (**3**), and the face-sharing bioctahedral chromium(III) compounds $\{Me_5C_5Cr\}_2(\mu\text{-}CH_3)_2(\mu\text{-}CH_2)$ (**6***, **6**) and $[\{Me_5C_5Cr\}_2(\mu\text{-}CH_3)_3]^+$ (**7***, **7**) have been studied MO-theoretically by the extended Hückel method. Proceeding from **2** over **3** to **4***, or from **6*** to **7*** a 3-center/4-electron chloride or methylene bridge is replaced by a 3-center/2-electron methyl group (a methylidyne cap in the trimer). The 3c/2e bridges give rise to an increased metal–metal overlap population due to Cr–Cr bonding within the core levels. In the series of **2**–**3**–**4*** this is accompanied by a decrease in the Cr–Cr distance (329–284–260 pm) and effective magnetic moment, μ_{eff} (2.53–2.05–1.53 μ_B per Cr at room temp.). The latter can be ascribed to an increased splitting within the chromium d-block because of the shorter metal-metal separation. The bioctahedra **6*** and **7*** feature even shorter Cr–Cr contacts than **4*** (239 and 242 pm), primarily because of their face-sharing geometry. However, their effective magnetic moments (per Cr) are 2.33 and 1.32 μ_B at room temp. The high magnetic moment for **6*** can be understood from the orbital interactions in the frontier orbital metal d block: A face-sharing bioctahedron shows one σ, two δ, and no π type overlap, while an edge-sharing bioctahedron (**4**) has σ, π, and δ interaction between the metals. In the former this destabilizes only σ* sufficiently to prevent occupation by electrons (leaving five orbitals for six electrons, possible spin multiplicities S = 0, 1, 2) while for the latter both σ* and π* are destabilized beyond electron occupation (leaving four MOs for six electrons, possible spin multiplicities S = 0, 1). **4***, **6*** and **7*** are unusual examples of metal–metal bonded complexes containing octahedral Cr^{III} ions.

The subject of metal–metal bonding in transition metal dimers, trimers, clusters, and one-dimensional chains – ranging from single to quadruple bonds – is of special interest in the area of inorganic chemistry[1,2]. Quadruple bonds in dichromium(II) tetracarboxylate complexes are an area of intense theoretical[1,3,4] and experimental studies. The Cr–Cr distances in these tetracarboxylates of the general formula $Cr_2(RCO_2)_4L_2$ range from 228 to 254 pm[1,3]. With chromium in the oxidation state II (d^4-d^4) – or eight d electrons available – we can readily assign a Cr–Cr quadruple bond to the tetracarboxylates from an MO-interaction diagram of two corner-sharing octahedra (not shown here; see for example ref.[1]).

On the other hand, dinuclear chromium(III) (d^3) complexes should also have bond orders of three based e.g. on a $\sigma^2\pi^2\delta^2$ configuration in the case of an edge-sharing bioctahedron whose schematic orbital diagram is given in Figure 1. An edge-sharing bioctahedron represents one example of joining octahedra in a dinuclear complex.

So far however, di- (or poly-)nuclear chromium(III) complexes (d^3-d^3) were almost always found to exhibit repulsive interactions between the metal atoms (Cr–Cr > 300 pm)[5]. The majority of these chromium compounds feature two bridging groups between the metals as shown in **1**.

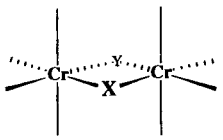

1

The d-d orbital diagram of a bioctahedral dimer derives from an interaction of the t_{2g} and e_g levels of both monomeric units to give t_{2g}-bonding and antibonding (t_{2g}^*), and e_g-bonding and antibonding (e_g^*) combinations as illustrated in Figure 1 for the edge-sharing case. The mixing in of the empty s and p levels (hybridization) has been omitted for simplicity. Of course, the actual position of σ (above or below π) depends on the ligand field and the metal–metal distance[6]. Throughout the following we will refer to σ-, π- and δ-type orbitals (rather than using the d_{xy}, d_{xz}, ... notation) to characterize the metal-metal interaction. We do not mean to imply a strict energy ordering for the orbitals or their dispersion between bonding and antibonding levels in Figure 1. The orbital energy ordering is rather schematic and can

  0009–2940/93/0303–0631 $ 10.00+.25/0

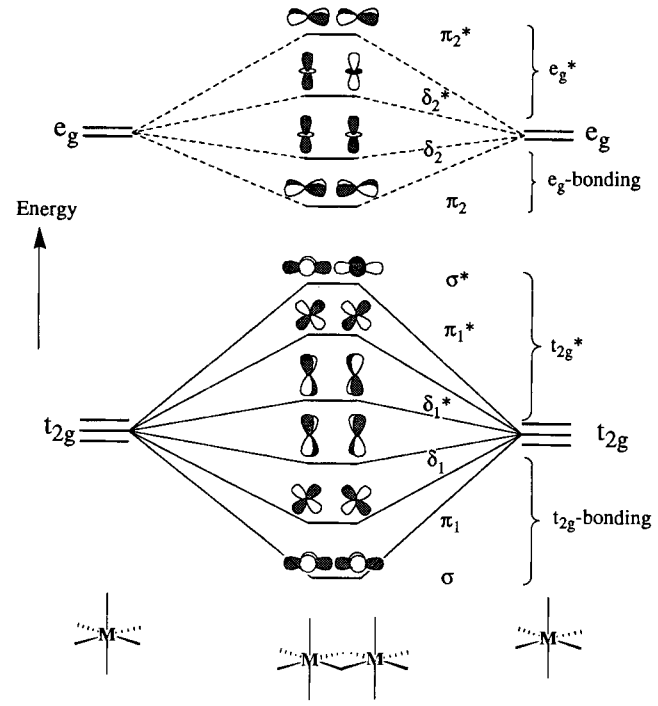

Figure 1. Schematic interaction diagram of two octahedral fragments in an edge-sharing bioctahedron. A 6-below-4 pattern emerges from the interaction of the t_{2g} and e_g levels giving t_{2g} bonding and antibonding below e_g bonding and antibonding

only be a rough first approximation. We realize however, that the 18-electron rule does not exclude a metal-metal bond in dichromium(III) systems. As we shall see in more detail later, it is a bridging geometry as in **1** that does not necessarily favor metal–metal bonding.

First, however, we will introduce a series of structurally characterized Cr^{III} complexes (**2**–**4*** and **6***, **7***; **2** denotes a compound containing the C_5H_5 ligand, while **4*** stands for a compound with the C_5Me_5 group)[7,8–10] which serve as illustrative examples for our discussion on metal–metal bonding in chromium(III) complexes. This analysis was undertaken in an attempt to rationalize the observed decrease of the Cr–Cr distances in this series.

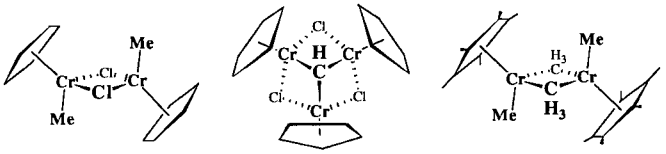

Cr-Cr = 329 282 261 pm

2 3 4, 4*

The conceptual change that transforms **2** into **4/4*** in a stepwise manner is the replacement of 3-center/4-electron chloride by 3-center/2-electron methyl bridges. In this progression we can think of the trimer **3** as representing the halfway point **3a**. The justification for this conceptual substitution is given in illustration **5** (Cp ligands omitted for clarity). The CH^{3-} fragment has six electrons (three electron pairs) available to contribute to three Cr–Cr bonds, or two electrons per Cr–Cr bond, analogous to the contribution of one bridging methyl group in **4**.

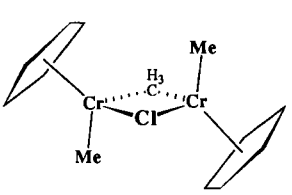

3a

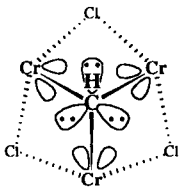

5

In light of the rather short Cr–Cr distance of **4*** (260.6 pm)[8], which approaches the upper limit of distances found in the quadruply bonded tetracarboxylates, the question arises, whether the assignment of a repulsive Cr^{III}–Cr^{III} interaction is still valid in this case. Alternatively, **4*** might be considered an example of a metal–metal bonded compound with trivalent chromium atoms.

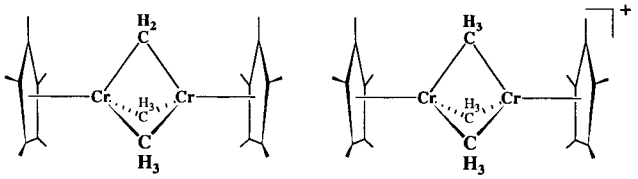

Cr-Cr = 239 242 pm

6, 6* 7, 7*

This last point was taken further with the structures of two related face-sharing bioctahedra, **6***[9] and **7***[10]. In the μ-methylene complex $[(\eta^5\text{-Cp*})Cr(\mu\text{-}CH_3)]_2(\mu\text{-}CH_2)$ (**6***) the Cr–Cr distance has collapsed to 239 pm, removing any doubts about a direct metal–metal interaction, as this value falls right in the range found in binuclear Cr^{II} carboxylates (see above). The μ-methylene complex **6*** once again contains a 3-center/4-electron bridge (i.e. the CH_2 group) which can formally be replaced again by a 3c/2e methyl bridge to yield the dinuclear cationic complex $[(\eta^5\text{-Cp*})_2Cr_2(\mu\text{-}CH_3)_3]^+[BF_4]^- \times CH_2Cl_2$ (**7***)[10], which then contains three bridging methyl groups connecting the chromium atoms. Contrary to initial expectations, the Cr–Cr distance of **7*** (242 pm) is slightly longer than that of **6***.

Magnetic Behavior

Compounds **2**, **3** and **4*** were prepared and characterized as part of a systematic study of the reactivity of paramagnetic chromium(III) alkyls[11]. The effective magnetic moment (μ_{eff}) per chromium atom of $[(\eta^5\text{-Cp})(CH_3)Cr(\mu\text{-Cl})]_2$ (**2**) as derived from magnetic susceptibility measurements was seen to increase with temperature and reaches a value of 2.53 μ_B at room temperature[7], which may be in contrast to the spin-only moment of 3.87 μ_B expected of an isolated S = 3/2 ion like Cr^{III}. This behavior is characteristic of antiferromagnetic coupling between the metal centers[12], which is presumably mediated by the bridging ligands.

In the methylidyne-capped trinuclear complex $[(\eta^5\text{-Cp})Cr(\mu\text{-Cl})]_3(\mu_3\text{-CH})$ (**3**) μ_{eff} per chromium atom increases

with temperature and reaches a value of 2.05 μ_B at room temperature[7]. While this behavior is certainly still consistent with antiferromagnetic coupling, the lower moment indicates a stronger interaction between the chromium atoms in **3** as compared to **2**.

Finally, the dimer $[(\eta^5\text{-Cp}^*)(CH_3)Cr(\mu\text{-}CH_3)]_2$ (**4***) still exhibits unpaired electrons, but the magnetic moment per chromium is much lower than in either **2** or **3**, reaching a value of ca. 1.48 μ_B at room temperature[8]. Based on the short Cr–Cr distance, the unusually small effective magnetic moment, and the results of electronic structure calculations (see below), we conclude that **4*** exhibits metal–metal bonding between two octahedral Cr^{III} ions.

The extremely short Cr–Cr distance of **6*** might have been expected to lead to extensive pairing of the d electrons in bonding molecular orbitals, and thus we were surprised to find that the effective magnetic moment per chromium atom of **6*** (2.33 μ_B at room temperature[9]), substantially exceeds that of **4*** and even **3**. However, the structural change from an edge-sharing to a confacial bioctahedron affects interaction of the d orbitals available for metal-metal bonding (see below). Thus, we believe that **6*** too features a $Cr^{III}-Cr^{III}$ bond.

Despite the very similar molecular structure of **6*** and **7*** the magnetic behavior of **7*** is consistent with a very strong metal–metal interaction. The temperature dependence of μ_{eff} features a steadily rising moment reaching 1.32 μ_B per chromium atom at room temperature[10] being the smallest value for all five compounds that have been compared here[13].

Electronic Structure and Bonding

We now turn to an analysis of the influence of bridging ligands on the electronic structure and consider the possibility of $Cr^{III}-Cr^{III}$ bonding in complexes **2**–**4** and **6**, **7**.

The reader's attention is also drawn to a seminal paper by Hoffmann et al. on bridged and unbridged M_2L_{10} complexes whose basic philosophy was very inspiring to our analysis[6].

4-Electron versus 2-Electron Bridges: The 3-center/2-electron (3c/2e) bonding mode is often found in so-called "electron-deficient" molecules, such as boranes[14], methyl-bridged aluminum dimers (e.g. **12**, **13**)[15] and hydrogen-bridged osmium trimers (e.g. **15**, **16**)[16]. The molecular orbital picture of two 3c/2e bridges is shown in **10**. The in-phase combinations of metal orbitals with the bridging ligand orbitals correspond to two MOs with metal-metal bonding character, one of σ and the other of π-type. For comparison, the picture for two 3-center/4-electron (3c/4e) bridges is shown in **8**. With the additional four electrons we can fill two more metal–ligand bonding orbitals; however, both of these are metal–metal antibonding in character. The net effect is an antibonding metal–metal interaction. Compounds with one 3c/2e and one 3c/4e bridge lie between these extremes and retain partial metal–metal bonding character, since only one metal-metal antibonding MO is filled as depicted in **9**.

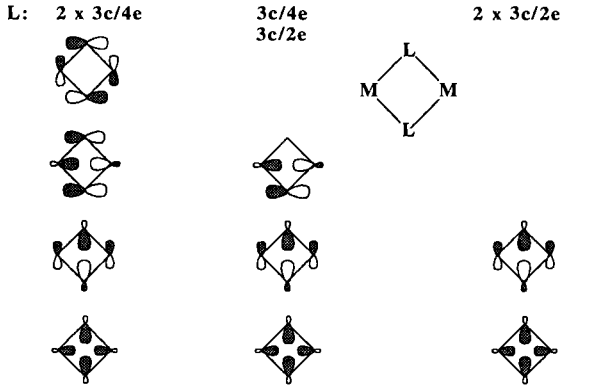

8 **9** **10**

In summary, metal–metal bonding can result from the presence of 3-center/2-electron bridges. As 4-electron bridges are replaced by 2-electron bridges, a metal–metal antibonding interaction (**8**) is transformed first to a single metal–metal bond (**9**) and finally to a metal–metal double bond (**10**). Such progressions are seen and accompanied by a decrease in the metal-metal distance, for example, in series of aluminium compounds (**11**–**13**)[17] or trinuclear osmium clusters (**14**–**16**)[16].

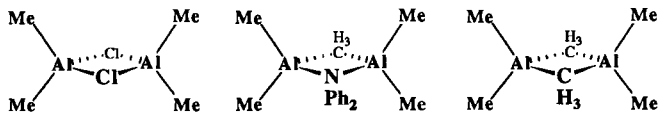

Al-Al = 322 272 261 pm

11 **12** **13**

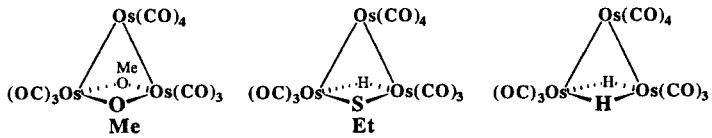

Os-Os(bridged) = 308 286 267 pm

14 **15** **16**

Returning to the series of Cr^{III} complexes (**2**–**4***), we can recognize the progressive shortening of the Cr–Cr distances as a consequence of increasing metal–metal bonding associated with the 3c/2e methyl bridges. The long Cr–Cr distance in **2** can be interpreted as being due to metal–metal repulsion according to **8**. Trinuclear **3** with its methylidyne and chloride exemplifies the intermediate situation **9**. We have shown earlier how the valence orbitals of two Cp(Me)Cr fragments and the sp^3 hybrid orbitals of two bridging methyl groups give rise to a Cr–Cr σ and π bond for **4** within the core levels[8].

We can also follow the change in "bond order" from **2** over **3a** to **4** using overlap populations. Neglecting for now the influence of the frontier d orbitals and computing

Cr–Cr overlap populations due to core orbitals only, we find: $\mathbf{2}^{6+}$, 0.045; $\mathbf{3a}^{6+}$, 0.115; $\mathbf{4}^{6+}$, 0.186[18]. It is also interesting to note the similarity in the trend of the bridging parameters (metal–metal distance, $M-C_{bridge}-M$ angle) between the chromium complexes **2**–**4*** and the series of aluminium dimers **11**–**13**[17].

The Chromium Frontier Orbitals – An MO Calculation

While metal–metal bonding due to 3c/2e bridges is surely important in **4**, this core level effect is probably not solely responsible for its short metal–metal separation. The following analysis will show that the 3c/2e bridges induce a change in the interactions of the Cr d orbitals from repulsive to bonding. Finally, possible steric effects of methyl or methylidyne bridges will be discussed.

The chromium complexes discussed herein differ from the aluminium compounds **11**–**13** by their partially filled frontier d orbitals. These orbitals afford the capability for multiple metal–metal bonding. However, if the bonding and antibonding d orbital combinations are very close in energy – i.e. within ca. 1 eV – metal–metal bonding due to the d block will depend critically on the electronic configuration, the extremes being low-spin and high-spin configurations. According to Figure 1 it is, of course, the t_{2g}-bonding and antibonding set that we mean when we speak about the orbitals of the d block. The e_g sets are too high in energy to play a role in the Cr–Cr interaction. An important factor in determining the splitting between the bonding (t_{2g}) and antibonding (t_{2g}^*) levels is the size (or diffuseness) of the metal orbitals involved. This is nicely illustrated by the series of $M_2^{III}Cl_9^{3-}$ ions of group 6, **17**–**19**[19–21].

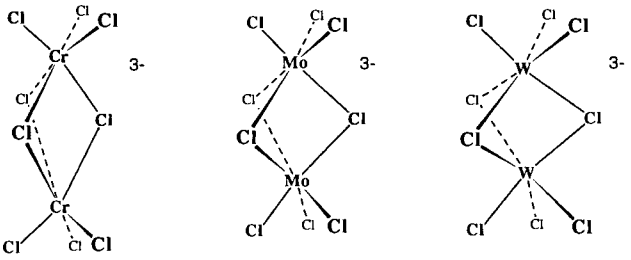

17 18 19

All are isoelectronic d^3-d^3 dimers, but in $Cr_2Cl_9^{3-}$ the contracted Cr 3d orbitals allow only for weak overlap and hence a small t_{2g}-t_{2g}^* splitting. Antiferromagnetic coupling – i.e. an equilibrium of various spin states (S = 0, 1, 2, 3) – is the result and leads to metal–metal repulsion (physical evidence for the latter is a Cr–Cr distance which is longer than the distance between the midpoints of the two octahedra described by the chloride ligands)[19–21]. The larger $t_{2g}-t_{2g}^*$ splitting in $Mo_2Cl_9^{3-}$ due to the larger and more diffuse molybdenum 4d orbitals effects pairing of two electrons in a metal–metal bond[22]. The tungsten complex with its most diffuse and largest 5d orbitals exhibits the greatest d-d overlap in this series; consequently, it has the largest splitting and all six electrons are paired in a low-spin state to form a metal–metal triple bond. The increase in metal–metal bonding from **17** to **19** is nicely paralleled by the decrease of the M–M distances.

In the bridged chromium dimers **2**, **3**, and **4***, we will have to deal with small splittings between the bonding and antibonding frontier orbitals and the distinctive possibility of high-spin configurations (this is the reason for the popularity of $Cr^{III}-Cr^{III}$ systems for studies of magnetic interactions).

In the following we describe the results of molecular orbital calculations carried out on the chromium alkyls described above. The computations were performed within the framework of a one-electron theory, namely that featuring an extended Hückel Hamiltonian[23]. Because this method does not explicitly include electron-electron interactions, we cannot expect these calculations to account quantitatively[24–26] for the observed magnetic properties of the molecules. However, we aim at a description of the orbital structure of the three complexes and wish to discuss on the basis of overlap, symmetry and relative orbital energy – all these factors being reasonably well handled by the extended Hückel method – the structures (especially Cr–Cr distances) adopted by the various compounds. The relevant geometrical and computational details may be found in the Appendix.

The dinuclear complexes **2**, **3a**, and **4** may be viewed as the union of two octahedra sharing an edge (see **20**). Each individual octahedron possesses the usual 3-below-2 orbital pattern shown in Figure 1. The formation of **20** simply involves the construction of linear combinations with C_{2h} symmetry of these levels as depicted in Figure 1 as well.

20

The Chloride-Bridged Dimer **2** *– Reversal of the "Natural" Energy Ordering:* The lowest six d orbitals of **2** according to a calculation are shown in Figure 2 (**a**). The topology of these MOs is not unexpected (cf. Figure 1) and we find the bonding and antibonding combinations of the σ, π and δ type. The important features of Figure 2 (**a**) are (i) the clustering of the six states within ca. 1 eV, and (ii) the relative energy ordering of the levels and their bonding or antibonding nature with respect to the two metal atoms.

The small dispersion of the levels follows directly from the large Cr–Cr distance of 329 pm, which allows only weak overlap between the chromium d orbitals. This distance is typical of polynuclear chromium(III) complexes with bridging chloride ligands and consistent with the absence of any metal–metal bonding[27]. Concerning the relative energies, it is clear that the "natural" ordering – i.e. bonding-below-antibonding – of the d combinations is not realized for the δ sets: $1a_u$ (δ*) lies below $1b_g$(δ) in energy. The same is true for π and π*, although for these levels the

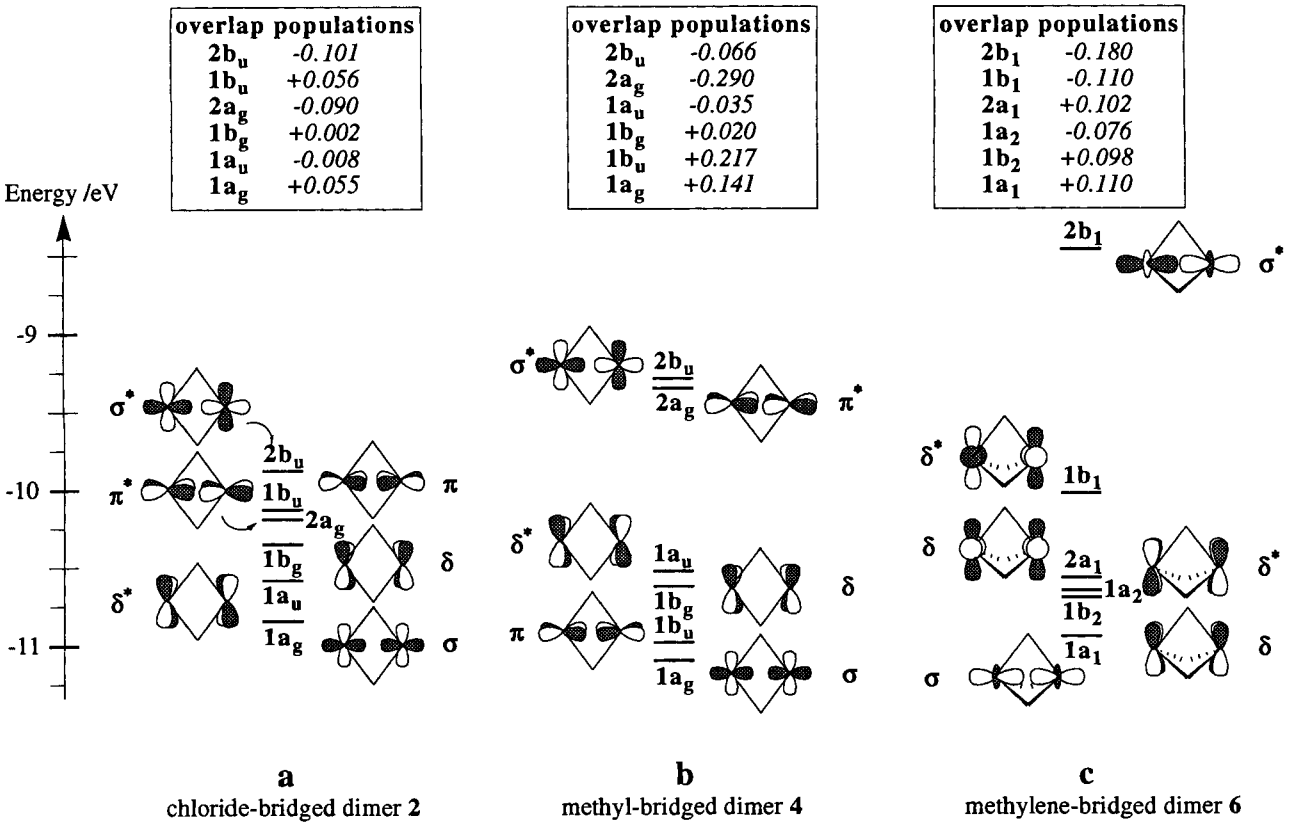

Figure 2. Frontier d orbitals of the edge-sharing chloride-bridged dimer **2** (**a**), the methyl-bridged chromium dimer **4** (**b**) and face-sharing μ-methylene-bridged dimer **6** (**c**); each filled with six electrons. The overlap populations for these orbitals were calculated for doubly occupied levels. Note the reversal of the "natural" energy ordering in **a** for the δ and π levels by a through-bond coupling effect and the clustering of six orbitals within ca. 1 eV because of the large Cr–Cr distance. In **b** the σ* and π* levels are separated from the four lower orbitals by about 1.5 eV. Symmetry labels were assigned by assuming C_{2h} symmetry for **2** and **4**, respectively C_{2v} for **6**

ordering is easily reversed with slight changes in geometry. Despite the small energy differences involved and the approximate nature of our calculations we think that these features are real, since they emerge as direct consequences of symmetry and overlap factors. Because of their local nodal properties orbitals $1b_g$ (δ) and $1b_u$ (π) contain an appreciable amount of chloride p character, see **21**, $1a_u$ (δ*) and $2a_g$ (π*) on the other hand do not suffer a similar destabilization by π antibonding with the bridges, since that would require filled d orbitals on the Cl atoms.

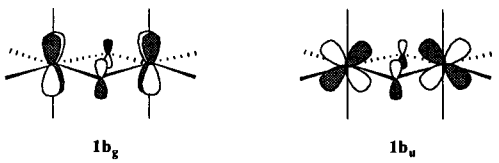

21

This through-bond coupling effect has been analyzed in detail by Hoffmann and co-workers for molecular[28] and extended[29] edge-sharing tetrahedral systems. In all cases the net result is that for long M–M distances the metal-metal bonding MO is shifted upward in energy relative to its antibonding counterpart.

Dimer **2** is a d^3-d^3 system: thus a total of six electrons must be accommodated in the d block of the complex and owing to the small energetic splitting of the t_{2g}-derived levels various configurations and spin states will arise. The molecule may assume four spin states, namely a singlet (S = 0), a triplet (S = 1), a quintet (S = 2), and a septet (S = 3). The calculation of the coefficients for all possible 6-electron configurations lies beyond the reach of our computational tool. The structure displayed by **2** is dictated by the various contributions of different spin states to the spin equilibrium. Only the S = 3 state (high-spin form) is pure in the sense that it results from only one configuration (all MOs singly occupied by α or β spins). The fact that this state contributes significantly to the long Cr-Cr distance may be gleaned from an examination of the variation of the sum of orbital energies as a function of change in the Cr–Cr distance. Figure 3 shows a Walsh diagram for the breathing motion depicted in **22**, and superimposed onto it, is the sum of the orbital energies for the S = 3 and S = 0 states. For the curve describing the latter, a two-electron occupation of the lowest three MOs was used.

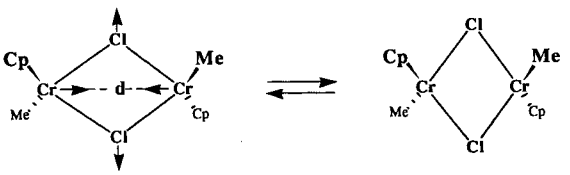

22

The energetic behavior of each of the six d-centered levels represented in the figure is easy to understand: As d(Cr – Cr) decreases, direct metal – metal overlap pushes the strongly bonding ones low in energy ($\sigma \equiv 1a_g$, $\pi \equiv 2b_u/1b_u$) and destabilizes their antibonding counterparts ($\sigma^* \equiv 1b_u/2b_u$, $\pi^* \equiv 2a_g$). Within this range of distance, the δ type MOs remain essentially unaltered. The total energy curve for S = 0 follows the trend dictated by $1a_g$ and $1b_u$. Reversibly, S = 3 is dominated by the changes in $2b_u$ and $2a_g$. Note that the sum of orbital energies does not depend on the spin of the electrons occupying these MOs. More specifically, configurations which feature unpaired electrons with opposite spins (for lower spin states) will contribute, in terms of the orbital energies, to a stabilization of the long Cr – Cr distance geometry.

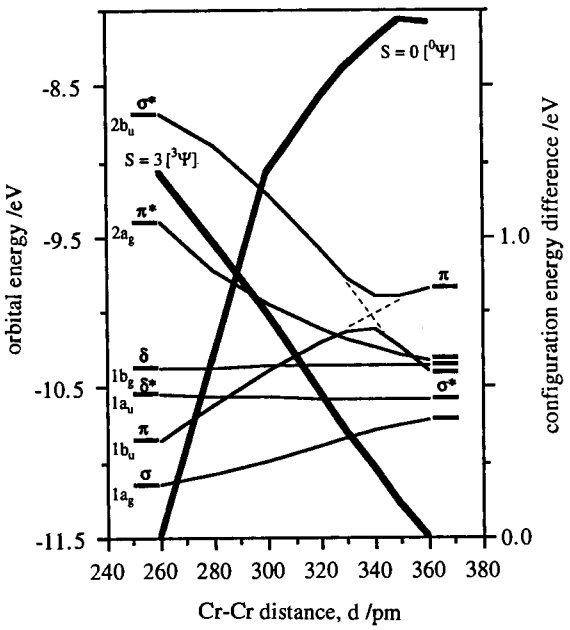

Figure 3. Walsh diagram for the breathing motion in the chloride-bridged dimer **2** (cf. **22**). The d-block orbitals are sketched in Figure 2 (**a**). The two thick lines represent the relative variation of the sum of orbital energies for two specific configurations and refer to the right-hand axis. The dashed lines help to visualize an avoided crossing. Note how a high-spin configuration (S = 3) contributes to a long Cr – Cr distance (the experimentally determined metal separation is 329 pm)

The above analysis was aimed at a semi-quantitative description of the Cr – Cr interaction in the chloride-bridged dimer **2**. The availability of various spin states results in a repulsive interaction between the two metal atoms and gives rise to an overlap population which is either vanishingly small or negative. Thus, it appears that octahedrally coordinated Cr^{III} ions show little propensity to form covalent bonds between each other. The large overlap between t_{2g}-derived d orbitals, which is required for bond formation, must be possible only at very short distances normally prohibited by core-core repulsions. However, under very special circumstances – e.g. in the presence of core-core attractions due to 3-center/2-electron bridges – the chromium atoms may move close enough together to lead to substantial overlap and splitting of the d orbitals and thus make Cr – Cr bonding possible (see below).

The Methyl-Bridged Dimer **4**: The frontier d orbitals of **4** resulting from a calculation were shown in detail in Figure 2 (**b**). Their energy ordering is what we would consider normal, with σ below π, π below δ etc. However, this time the Cr d orbitals are spread over 1.8 eV.

Again the extent of Cr – Cr bonding depends strongly on the assignment of electrons to levels, i.e. the electron configuration. The low-spin configuration (spin angular momentum, S = 0) $^0\Psi \equiv (1a_g)^2(1b_u)^2(1b_g)^2$ with all electrons paired in the lower three Cr – Cr bonding orbitals is strongly bonding (total d block overlap population 0.378), while the high-spin state (S = 3) $^3\Psi \equiv (1a_g)^1(1b_u)^1(1b_g)^1(1a_u)^1(2a_g)^1(2b_u)^1$ is nonbonding (–0.007 overlap population). However, due to the large energy gap between the $1a_u$ and $2a_g$ levels we suggest that only the four lowest levels are energetically accessible for **4**, leading to a singlet-triplet equilibrium. This hypothesis is consistent with the low magnetic moment of **4***.

Once again, however, the two states must be described by linear combinations of 6-electron configurations (Slater determinants) and the calculation of the coefficients associated with these linear combinations is impossible with our method. But we can give an upper and lower bound by looking at the configurations which contribute to the singlet and triplet states. The four configurations for the S = 0 state[30] and the six for the S = 1 state are listed in Table 1 along with their contributions to the Cr – Cr overlap population of **4**. All configurations contribute to Cr – Cr bonding and most of them do so very strongly. While the splitting of its d orbitals is not sufficient to enforce pairing of all electrons in a triply bonded and thus diamagnetic molecule, **4** nevertheless emerges as an unusual example of metal – metal bonding between octahedral Cr^{III} ions.

Table 1. Contributions of the S = 0 and S = 1 d-block configurations to the Cr – Cr d overlap population in the methyl-bridged dimer **4**

Configurations (S = 0)	Cr – Cr d overlap population
$(1a_g)^2(1b_u)^2(1b_g)^2$	0.378
$(1a_g)^2(1b_u)^2(1a_u)^2$	0.323
$(1a_g)^2(1b_g)^2(1a_u)^2$	0.126
$(1b_u)^2(1b_g)^2(1a_u)^2$	0.202
Configurations (S = 1)	
$(1a_g)^2(1b_u)^2(1b_g)^1(1a_u)^1$	0.350
$(1a_g)^2(1b_u)^1(1b_g)^2(1a_u)^1$	0.252
$(1a_g)^1(1b_u)^2(1b_g)^2(1a_u)^1$	0.290
$(1a_g)^2(1b_u)^1(1b_g)^1(1a_u)^2$	0.225
$(1a_g)^1(1b_u)^2(1b_g)^1(1a_u)^2$	0.263
$(1a_g)^1(1b_u)^1(1b_g)^2(1a_u)^2$	0.165

The Electronic Structure of the Trimer **3**: In the following, we describe the electronic structure of the trimer **3** and wish to discuss on the basis of our calculations the type of interaction that exist between the Cr atoms in this system. Complex **3** belongs to a class of compounds – trinuclear clusters of early transition metals – for which various orbital descriptions have been recently provided[31]. It could be shown

that the extended Hückel and SCF Xα-SW method agree well in their bonding description (relative MO energy ordering) for Cp_3M_3-type clusters[31b]. Yet, **3** seems to be somewhat unusual since it features d^3-Cr atoms, formally surrounded by an octahedrally arranged set of ligands, within what is believed to be a bonding distance. As mentioned earlier, trinuclear clusters of this type with metal–metal bonds do exist, but with atoms not being chromium. Systems which involve Cr atoms so far have displayed only long (>320 pm) intermetallic distances[32]. Yet, the mean Cr–Cr distance of 282 pm in **3** falls well within the accepted range of Cr–Cr single bonds[33]. Counting each Cp^- and Cl^- as uninegative and the C–H cap as −3, we characterize the trimer **3** as a d^3-d^3-d^3 system. One may therefore envision three distinct possibilities, schematically represented in **23a–c**, of organizing the 9 electrons. In **23a** (only one resonance form is shown), eight of them are paired up to generate three σ and one π bond. The magnetic data presented in an earlier section are inconsistent with one unpaired electron so that **23a** is ruled out. Similarly, **23b** would possess three σ bonds and a total of three unpaired electrons: An S = 1/2, S = 3/2 spin equilibrium would result and the room-temperature magnetic moment that we observe tells us that **23b** must be discarded[34]. There remains **23c** with no metal-metal bond (derived from the frontier orbitals) and the possibility of a spin equilibrium between S = 1/2, S = 3/2, S = 5/2, S = 7/2, S = 9/2 spin states. The magnetic data can accommodate such a possibility, but the short Cr–Cr distances now become a puzzle since, interpreted at face value, they imply the existence of spin pairing in covalent bond orbitals, as in **23b**.

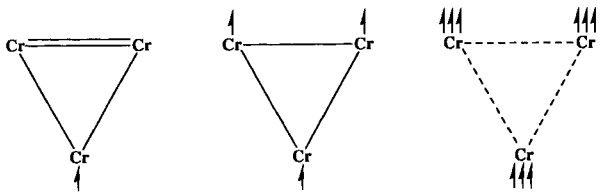

23

We begin with a rapid description of the electronic structure of **3**. The orbital structure of this type of complex may be derived in several ways, and Figure 4 shows one manner of doing so, primarily on the basis of symmetry considerations. The starting point [Figure 4 (**a**), extreme left] is the splitting pattern resulting from the assemblage of a metal with a Cp ligand. These fragment orbitals have been described at length elsewhere[35] and suffice it to say that one finds a t_{2g}-like set, followed higher in energy by an e set (remnant of the octahedron e_g set) strongly hybridized away from Cp, and then an sp hybrid of cylindrical symmetry. Taking C_{3v} symmetry-adapted combinations[36] of these six fragment MOs, we can generate for each of them either an $\{a_1 + e\}$ or an $\{a_2 + e\}$ set[37], as indicated in Figure 4 (**b**). The actual complex **3** is of lower C_s symmetry. The symmetrization employed here which consists in a 180° rotation of one Cp ligand only simplifies but does not fundamentally alter the interaction diagram. Now, turning to the right-hand side of Figure 4 (**d**), each chloride will present three p orbitals which can interact with the d block. Figure 4 (**d**) combines in C_{3v} symmetry the nine p functions of three briding chlorides. The two a_1 and the a_2 combination are shown in **24** (no significant sp hybridization is observed).

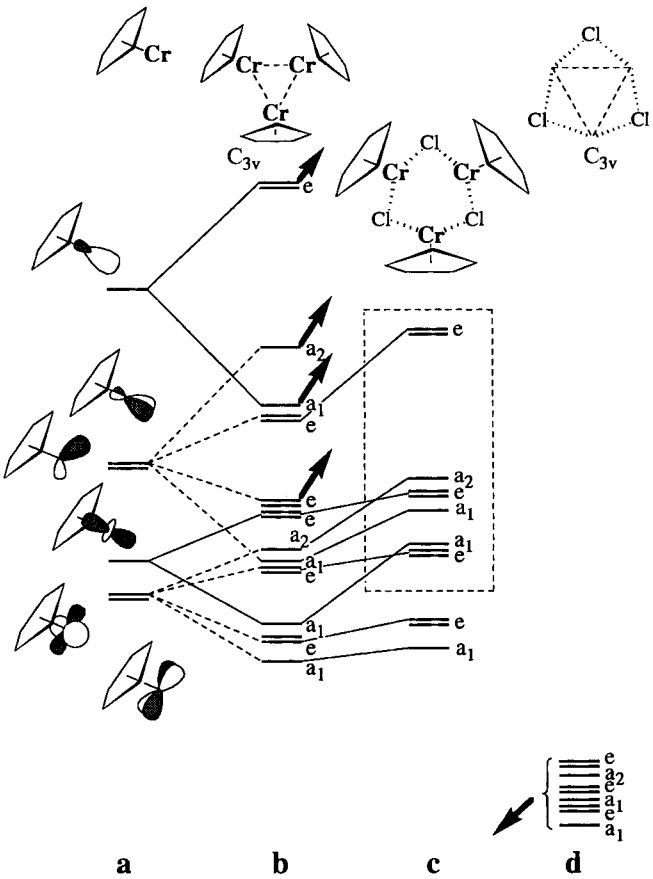

Figure 4. Constitution of the molecular orbital scheme for the trimer **3** without the μ-CH cap; see text. Symmetry labels were assigned in C_{3v} symmetry

Regardless of the exact magnitudes of the interactions, the approximate MO structure of the trimer **3** minus the C–H cap, is then constructed on symmetry grounds: The two $\{a_1 + e\}$ and $\{a_2 + e\}$ sets of the Cl atoms will be pushed down by $\{a_1 + e\}$ and $\{a_2 + e\}$ sets of the trinuclear core. This is summarized by the arrows in Figure 4. What we are left with for the fragment in Figure 4 (**c**), ready to interact with the μ^3-CH cap, are the various orbitals boxed-in with a dashed line in Figure 4 (**c**) and an $\{a_1 + e\}$ set directly below. The cap offers an $\{a_1 + e\}$ set (see **25**) which

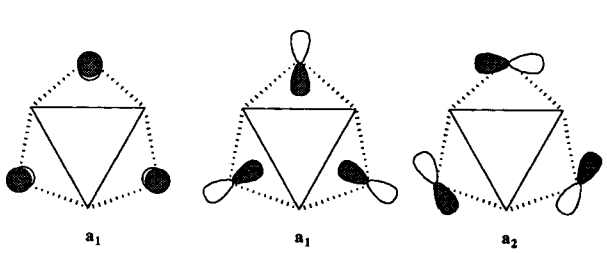

24

interacts mostly with the just mentioned lower $\{a_1 + e\}$ set in Figure 4 (c) to form the three Cr–C σ bonds. The boxed-in orbitals are even slightly stabilized to give the d block frontier orbitals shown in **26**. As expected, the d block of the trimer **3** is constituted of 9 orbitals descending from the C_{3v} combination of three t_{2g} sets produced by the local octahedral environment of each of the Cr atoms.

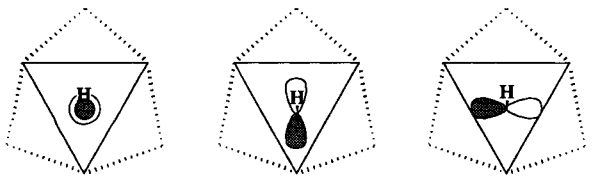

25

In **26** we show the splitting as it actually comes out of the calculation on **3** with the Cr–Cr distances set at the experimental geometry (282 pm).

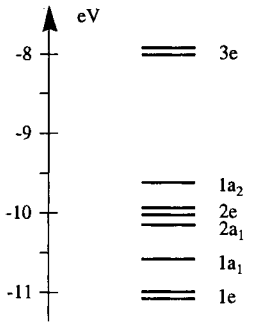

26

The overall pattern agrees well with that found by Jiang et al. in the geometrically analogous $Mo_3(\mu^2\text{-}Cl)Cl_9(\mu^3\text{-}S)$ cluster[31]. Owing to the packing of 7 levels (1e to $1a_2$) within less than 1.5 eV, the exact occupation of each level becomes again difficult to assert, and the existence of a spin equilibrium is all the more obvious. From the energy diagram shown in **26**, we believe that the contribution of states with spin S = 7/2 and S = 9/2 to such a spin equilibrium should be small due to the large energy gap between $1a_2$ and 3e (cf. to the orbital splitting of **4**). Hence, we do not take these configurations into account in the following. Having at most an S = 5/2 spin state agrees well with the experimental observation of a somewhat lower magnetic moment for **3** (2.05 μ_B at room temperature) as compared to **2** (2.53 μ_B) where S = 3 was the highest spin state accessible.

Configuration $^{1/2}\Psi$ represents in some way the case of structure **23a**. Would it solely contribute to the structural choice made by the trimer, shorter Cr–Cr distances would be observed. This was tested by allowing the trimer to relax and contract from its equilibrium structure by varying the Cr–Cl–Cr and Cr–C(H)–Cr angles concurrent with a change in Cr–Cr separation. Figure 5 shows the sum of one-electron orbital energy variations as the trinuclear core shrinks or expands, for the configurations $^{1/2}\Psi$, $^{3/2}\Psi$, and $^{5/2}\Psi$.

Not unexpectedly, the minima are shifted towards long Cr–Cr distances as one goes from $^{1/2}\Psi$ to $^{5/2}\Psi$. The fact that the experimental distance lies close to the minimum of $^{5/2}\Psi$ is considered fortuitous. Yet, we believe it shows how the availability of high-spin states shifts upward the optimum Cr–Cr distance relative to what it would be if orbital energies were the only factor at work: just like in the dimer case **2**, little metal–metal d overlap allows population of Cr–Cr antibonding levels by unpaired spins. However, even after such a lengthy discussion we should not overestimate the frontier d orbital influence for the Cr–Cr bond length. We feel that they merely provide a fine-tuning and that for the most part the much smaller Cr–Cr distance observed for the trimer is the result of one 3c/2e bridge which provides a core metal–metal overlap population of 0.086 for **3**.

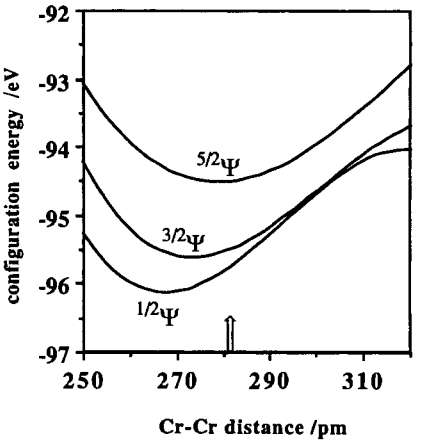

Figure 5. Variation of the sum of orbital energies for three specific configurations for the breathing motion in the methylidyne-capped chromium trimer **3** ($^{1/2}\Psi \equiv (1e)^4(1a_1)^2(2a_1)^2(2e)^1$; $^{3/2}\Psi \equiv (1e)^4(1a_1)^2(2a_1)^1(2e)^2$; $^{5/2}\Psi \equiv (1e)^4(1a_1)^1(2a_1)^1(2e)^2(1a_2)^1$). Note how high-spin configuration (S = 3/2 and 5/2) shift the minima towards long Cr–Cr distances. The arrow indicates the experimental distance of 282 pm

The Clamping Effect and Bridge-Bridge Repulsion: One might argue that in stressing the concept of 3c/2e versus 3c/4e bridges we may have overlooked the geometrical constraints imposed by the Cr–bridge bond lengths, bridge–bridge distances and/or Cr–bridge–Cr angles. The Cr–Cr distance might be largely determined by an optimization of the Cr–bridge–Cr angle in what could be called a "clamping effect" of the Cl and CH_3 bridges or the CH cap – thus forcing the chromium atoms together (or apart) (cf. ref.[6]).

A test of this hypothetical clamping effect must involve a determination whether the observed structures of **2**, **3**, and **4** coincide with those dictated solely by the Cr–bridge–Cr angles. We arrive at the predicted structures by minimizing the corresponding total energy. Because we are interested here in what could be called the "natural" bite angle of the bridges or cap, the numbers were computed on a system possessing no d electrons[6]. Thus, the optimum Cr–bridge–Cr angle is governed only by the low-lying Cr–C bonding MOs. Figure 6 summarizes the variations in total energy upon changing the Cr–Cr distances of $\mathbf{2}^{6+}$,

3^{9+}, 4^{6+} (cf. **22**, Figure 3) while keeping the Cr—bridge distances constant.

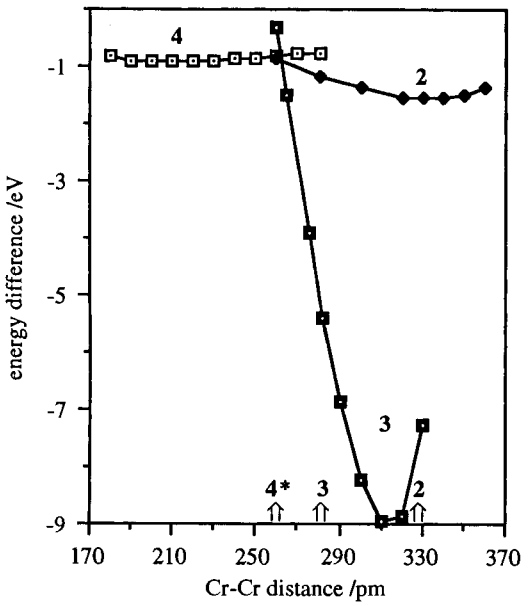

Figure 6. Variation in the total core level energy for 2^{6+}, 3^{9+}, and 4^{6+} as a function of Cr—bridge—Cr angle variation, concurrent with the Cr—Cr distance plotted as the abscissa (breathing mode, cf. **22**). The positive charge serves to remove the ambiguous contribution from the d-block frontier orbitals. The minima in total core level energy reflect a maximum in Cr—bridge bonding

The maximum amount of Cr—bridge bonding — corresponding to a minimum in total energy — for **2** is found for a geometry with a Cr—Cr distance of around 330 pm, i.e. approximately the experimental one. This is consistent with the expectation that in the absence of a strong Cr—Cr repulsion or attraction the Cr_2Cl_2 core geometry should be governed by the bridging constraints. For **4**, we calculate a rather shallow minimum, somewhat shorter than the experimental distance of 260 pm. Here we see that both core level effects — namely 3c/2e bridges and the clamping effect — work in the same direction; their relative importance is thus not easily discernable.

However, for **3** the energy optimization predicts a Cr—Cr distance or ≈315 pm (or alternatively an optimum Cr—C—Cr angle of ≈109°, coinciding with a tetrahedral environment for the methine carbon). This is appreciably larger than the 282 pm of the actual structure. Our interpretation of this result is that the structure of **3**, or more specifically the apparently bonding contacts between the Cr(+3) ions, result from the electronic consequences of a 3c/2e bridge overriding the Cr—C bond optimization (the clamping effect). Consequently, we conclude that for **4** also the electronic influence from the two 3c/2e bridges is much more important than a methyl clamping effect.

It is also illustrative to consider the geometrical consequences of a fixed Cr—bridge distance upon the Cr—Cr distances in these molecules. While structures **2** and **4** represent edge-sharing octahedra, **6** and **7** feature face-sharing ones. If we approximate the chromium-bridge core with a square at a fixed metal—bridge distance ***a***, the corresponding metal—metal and bridge—bridge contacts are given by $a\sqrt{2} = 1.414a$ in the edge-bridging bioctahedra. For the face-sharing bioctahedron with an idealized inner core (all bridge-metal-bridge angles 90°) the metal—metal separation is calculated as $2a/\sqrt{3} = 1.155a$, the bridge—bridge distance as $a\sqrt{2}$. In Table 2 the values for **2**, **4**, **6** and **7** calculated for an idealized core geometry are compared to the observed contacts.

One notes a good agreement or only slight distortion for **2**. The large differences (over 40 pm) between the observed distances and the calculated ones for the methyl-bridged dimer **4*** are striking. We are certain that a bridge-bridge repulsion cannot account for this distortion — at the idealized distance of 309 pm the bridge-bridge core-level overlap population is only −0.003. Rather, $\{Me_5C_5(Me)Cr(\mu\text{-}CH_3)\}_2$ (**4***) is an exceptional case of a Cr(III)—Cr(III) metal bond.

The μ-Methylene-Bridged Dimer **6**: **6*** features the shortest contact between two chromium(III) centers known to us to date. This Cr—Cr separation is even shorter than some Cr—Cr bond lengths found in the Cr(II) tetracarboxylates (range: 228 to 254 pm), which are generally assigned a Cr—Cr quadruple bond[1]. For such a short metal—metal distance one should expect a large splitting within the metal d block between bonding and antibonding levels, such that a diamagnetic complex might result. However, experimentally we find that **6*** has a larger magnetic moment than the closely related compound $\{Me_5C_5(Me)Cr(\mu\text{-}CH_3)\}_2$ (**4***), which exhibits a 20 pm longer Cr—Cr separation.

Based on a geometric calculation (Table 2; below and ref.[9]) it may seem unnecessary to invoke metal—metal bonding to explain the short contact in **6***. Rather, the metal—metal interaction may be viewed as the result of a

Table 2. Comparison between calculated and observed Cr—Cr and bridge—bridge distances for some chromium dimers

Compound		Cr—bridge[a] [pm]	Ideal, calculated Cr—Cr [pm]	Ideal, calculated bridge—bridge	Observed Cr—Cr [pm]	Observed bridge—bridge	Ref.
$\{C_5H_5(Me)Cr(\mu\text{-}Cl)\}_2$	**2**	235.6	333.2	333.2	328.7	337.6	[7]
$\{Me_5C_5(Me)Cr(\mu\text{-}CH_3)\}_2$	**4***	218.8	309.4	309.4	260.6	351.5	[8]
$\{Me_5C_5Cr\}_2(\mu\text{-}CH_3)_2(\mu\text{-}CH_2)$	**6***	204.0 (Cr-CH_2) 215.0 (Cr-CH_3)	244[b]	298[b]	239.4	301.6[a]	[9]
$[\{Me_5C_5Cr\}_2(\mu\text{-}CH_3)_3]^+$	**7***	217.6	251.3	307.7	242.3	312.9[a]	[10]

[a] Averaged values. — [b] Based on an averaged Cr—bridge contact of 211 pm.

short M–M contact. As in the molecular orbital study of **4**, we found earlier that the two 3c/2e methyl bridges play an important role in providing a strong metal–metal overlap population (0.206) from the core orbitals. Their metal-bridge bonding orbitals possess an inherent metal–metal bonding character[9]. The 3c/4e methylene bridge on the other hand has only a minor effect on the core level Cr–Cr overlap population, since its filled Cr–CH_2 bonding combinations also give rise to a metal–metal antibonding core level.

Qualitatively, a 6-below-4 pattern is found in general for confacial bioctahedra for the ten d levels – just as for an edge-sharing bioctahedron (cf. Figure 1). The lower six are split again with the details of the pattern, the magnitudes of the energy gap depending strongly on the metal and the M–X–M bridging angle[21,38,39]. In **6** (C_{2v} symmetry) the six chromium d frontier orbitals (the "t_{2g}-t_{2g}" interaction) present a metal-metal σ and two δ type overlaps with their bonding and antibonding combinations, shown in Figure 2 (**c**). The $2b_1$ σ* level, however, is too high in energy (1.5 eV above $1b_1$) to be populated in an electronic ground state. The remaining five levels lie within 1.0 eV and are filled with six electrons. Again, although the extended Hückel method[23] does not take into account electron-electron interactions and can thus not be expected to give a reliable prediction for the ground state of **6**, our calculation point to a mixture of singlet, triplet and pentet configurations entering the ground state. The contribution of these frontier orbitals to Cr–Cr bonding depends on the electron configuration chosen. Most configurations within each spin state ($^0\Psi$, $^1\Psi$, $^2\Psi$), are bonding and from the ten configurations contributing to $^0\Psi$[30] and the five of $^2\Psi$, we estimate the d contribution to the total Cr–Cr overlap population to be somewhat smaller than that from the core levels. The upper limit for the d block overlap population is 0.310 for $^0\Psi = (1a_1)^2(1b_2)^2(2a_1)^2$, the lower limit −0.088, set by $^0\Psi = (1b_2)^2(1a_2)^2(1b_1)^2$ upon populating antibonding levels.

Having two δ- and no π-type overlap in the ("t_{2g}") d block of two metal-centered face-sharing octahedra is, of course, the explanation for the high magnetic moment of **6*** when compared to **4***. **4** featured both σ and π bonding between the metals (cf. Figure 2), thus destabilizing both the σ* and π* levels beyond possible occupation, leaving only four MOs for 6 electrons (possible spin multiplicities S = 0, 1). However, **6** exhibits both σ and δ overlap and only the σ* orbital is destabilized sufficiently to prevent occupation by electrons, thus leaving five MOs to be filled with six electrons (possible spin multiplicities S = 0, 1, 2).

The Triply Methyl-Bridged Dimer **7**: The Cr–Cr bond in **6** was bridged by two 3c/2e methyl and one 3c/4e methylene bridge. We have emphasized that 3c/2e bridges play an important role in providing an inherent, strong metal–metal overlap population from core orbitals. Within this picture, one would expect the Cr–Cr core overlap population to increase and the M–M separation to decrease upon replacement of the 3c/4e methylene by a 3c/2e methyl bridge. However, while the metal-metal core overlap population indeed increases from 0.206 (**6**) to 0.249 (**7**) for the cyclopentadienyl model complexes, the measured Cr–Cr distance is slightly longer in **7*** (242 pm) than in **6*** (239 pm).

How can we understand this deviation between prediction and experiment? First, we have to contrast the experimental metal-metal contact with a theoretical value based on an ideal confacial geometry (all C–Cr–C = 90°, Cr–C–Cr = 70.5°) assuming an average Cr–C_{bridge} bond distance of 211 pm for **6** and 217.6 pm for **7**. Such a geometric calcu-

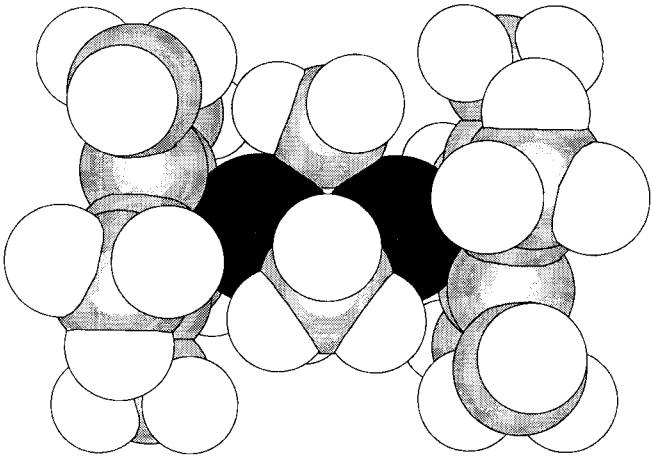

Figure 7. Space-filling plot of **7*** based on X-ray data[10]. Spheres for C and H are drawn at about 70% of the van-der-Waals radii. Note that the $methyl_{bridge}$–$methyl_{Cp}$ distance of 330–350 pm is less than the sum of their van-der-Waals radii (200 pm). The same is true for the $methyl_{bridge}$–$carbon_{Cp}$ distance of 310–330 pm (the half-thickness of an aromatic molecule is 170 pm). (van-der-Waals radii from L. Pauling, The Nature of the Chemical Bond, Cornell University Press: Ithaca, **1960**, NY, 3rd ed., p. 260)

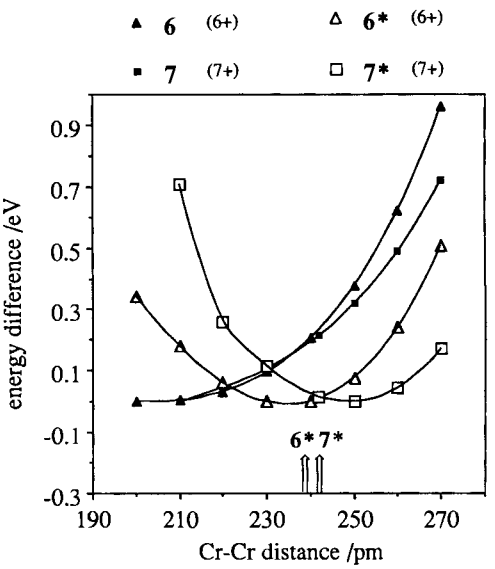

Figure 8. Variation in the total core level energy for the face-sharing bioctahedra $6^{6+}/7^{7+}$ with normal cyclopentadienyl and $6^{*6+}/7^{*7+}$ with pentamethylcyclopentadienyl as a function of Cr–bridge–Cr angle variation, concurrent with the Cr–Cr distance plotted as the abscissa (breathing mode, cf. **22**). The positive charge serves to remove the ambiguous contribution from the d-block frontier orbitals. The minima in the total core level energy for 6^{*6+} and 7^{*7+} reflect an optimization in Cr–bridge bonding and (μ-CH_3)-(Cp*-CH_3) repulsion. The arrows indicate the respective experimental Cr–Cr distances

lation (see Table 2) yields an anticipated Cr–Cr distance of 244 pm for **6** and 251 pm for **7**. Although the calculated value for **6** is somewhat uncertain due to the unsymmetric nature of the bridges, one can clearly argue that the Cr–Cr bond in **7*** is shortened (with respect to the ideal geometry) and relatively more so than in **6***.

While one would not necessarily invoke metal–metal bonding to explain the observed contact of 239, relative to 244 ppm in **6**, we feel the distance of 242 pm in **7*** has to be explained by a sizable metal–metal interaction, especially since the bond shortening seems to operate against a $methyl_{bridge}$–$methyl_{Cp^*}$ repulsion. A space-filling plot for **7*** in Figure 7 illustrates what is meant. We provide evidence for such a repulsion in Figure 8, which contains the variations in total core level energies as a function of Cr–Cr separation for $\mathbf{6}^{6+}$, $\mathbf{6^*}^{6+}$, $\mathbf{7}^{7+}$, and $\mathbf{7^*}^{7+}$ (**6**, **7*** being the *permethylated* Cp complexes). The energies were computed on systems possessing no d electrons to avoid a distortion through ambiguous d block occupation[6] (cf. the breathing modes of **2** to **4** in Figure 6). The Cr–bridge bond lengths were kept constant.

The cyclopentadienyl model complexes **6** and **7** do not show a relative minimum within the range of Cr–Cr distances plotted here. However, their permethylated parent complexes do. We can most easily understand these minima as the result of $methyl_{bridge}$–$methyl_{Cp^*}$ repulsions. For **6*** we calculate the minimum approximately at the experimentally observed Cr–Cr distance. Such a coincidence may be fortuitous, but in **7*** the calculated minimum lies clearly at larger Cr–Cr separation with respect to both its experimental value and the minimum for **6***. The shift to a longer metal–metal contact from **6*** to **7*** is understandable in the light of the replacement of a "flat" methylene by a "round" methyl group.

Therefore, the experimental Cr–Cr distance in **7*** of 242 pm has to be judged in the light of metal–metal bonding overcoming a strong $methyl_{bridge}$–$methyl_{Cp^*}$ repulsion, in addition to its longer "ideal" value of 251 pm. Looking ahead, we also conclude from Figure 8 that in the absence of $methyl_{bridge}$–$methyl_{Cp^*}$ repulsion still shorter Cr(III)–Cr(III) bonds may be possible, using either cyclopentadienyl instead of its permethylated analogue or by substituting smaller hydride ligands for the methyl bridges.

The interaction diagram for **7** (not shown) reveals only minor differences from the one for **6** (ref.[9]), most notably in the disappearance of the antibonding core levels stemming from the 3c/4e methylene bridge in **6**. In particular, the d-block splitting is very similar, thus, it fails to predict the dramatic reduction in μ_{eff} (**6***: 2.33 μ_B, **7***: 1.32 μ_B). Thus, we are forced to conclude that other factors (charge effects, counterion-mediated intermolecular exchange coupling?) play a role in determining its magnetic behavior. However, the low magnetic moment of **7*** does reinforce our notion of a strong metal–metal interaction.

With their 3c/2e methyl bridges the core level bonding in **6** and **7** is related to that in other confacial bioctahedra with two metals bridged by three hydrides such as $(p_3)Fe(\mu\text{-}H)_3Fe(p_3)^+$ (Fe–Fe = 233 pm, Fe–H–Fe = 79°), $(as_3)Co(\mu\text{-}H)_3Co(as_3)^+$ (Co–Co = 237 pm, Co–H–Co = 88°)[40] (with p_3, as_3 = $H_3C(CH_2PPh_2)_3$, $H_3C(CH_2AsPh_2)_3$) and $Me_5C_5Ir(\mu\text{-}H)_3IrC_5Me_5^+$ (Ir–Ir = 246 pm, Ir–H–Ir = 89.5°)[41]. Although the metal–metal distances in these compounds are quite short, a comparison of the M–H–M angles with the ideal value of 70.5°[19–21,38] shows that they are not compressed, as one would expect if a metal–metal bond were present. The bonding in these hydrido-bridged dimers has been analyzed previously[21] and the elongation traced to a geometrical preference for H–M–H angles smaller than 90°. In contrast to **6** and **7**, however, for d^6-d^6 systems (Fe–Fe, Ir–Ir) the six ("t_{2g}") frontier orbitals of a confacial bioctahedron are completely filled, contributing essentially nothing to metal–metal bonding[21].

Conclusions

The magnetic moments of a series of di- and trinuclear chromium(III) complexes (**2**, **3**, **4***, **6***) can be rationalized based on the splitting pattern of the frontier orbital metal d block. A one-electron MO approximation of the contributions of various spin states and configurations enables a qualitative interpretation of the changes in μ_{eff} within a series of edge-sharing chromium(III) dimers as the Cr–Cr contact is shortened (**2** over **3**/**3a** to **4**) and going from an edge- to a face-sharing bioctahedron (**4** to **6**). Fundamental to the decrease in the Cr–Cr distance in this series is the replacement of 3-center/4-electron (chloride) by 3-center/2-electron (methyl) bridges with their inherent metal–metal bonding character from the core levels. The methyl-bridged chromium(III) dimers $\{Me_5H_5Cr(CH_3)(\mu\text{-}CH_3)\}_2$ (**4***), $\{Me_5C_5Cr\}_2(\mu\text{-}CH_3)_2(\mu\text{-}CH_3)$ (**6***) and $[\{Me_5C_5Cr\}_2(\mu\text{-}CH_3)_3]^+$ (**7***) provide examples of metal–metal bonding between chromium atoms in the formal oxidation state +III, which hitherto has been thought to give rise only to repulsive metal–metal interactions.

Appendix

The calculations have been performed by using the extended Hückel method[23] including the weighted H_{ij} formula[42] for the evaluation of the H_{ij} term. The atomic parameters have been taken from previous work and are listed in Table 3. The calculations have employed idealized geometries closely approximating the experimental structures: **2**: Cr–Cr = 330, Cr–Cl = 236, Cr–C(Cp) = 224, Cr–C(Me) = 210, Cr–Cp(center) = 190.25, C–C(Cp) = 139 pm, Cr–Cr–C(Me) = 96.6°, Cr–Cr–Cp(center) = 140.14°; **3**: Cr–Cr = 282, Cr–C(cap) = 194, Cr–Cl = 236, Cr–C(Cp) = 219, Cr–Cp(center) = 183.235, C–C(Cp) = 141, C–H(cap) = 100 pm, Cp(center)–Cr–C(cap) = 130° (Note: The actual angle is closer to 120°, which, however, gives H(cap)–H(Cp) and H(Cp)–H(Cp′) contacts below 100 pm), C(cap)–Cr–Cl = 96.5°, C(cap)–Cr–Cr′–Cl = 180° (each chlorine lies in the plane formed by the two adjacent chromium atoms and the methine carbon). **4**: Cr–Cr = 260, Cr–C(bridge) = 220, Cr–C(terminal) = 210, Cr–C(Cp) = 230, Cr–Cp(center) = 195.2, C–C(Cp) = 143 pm,

Cr–Cr–C(terminal) = 94.2°, Cr–Cr–Cp(center) = 148.07°. **6**: Cr–Cr = 240, Cr–CH_2 = 204, Cr–CH_3 = 215, Cr–C(Cp) = 225.2, Cr–Cp(center) = 190.6, C–C(Cp) = 141 pm; idealized C_{2v} symmetry. **7**: Cr–Cr = 242, Cr–CH_3 = 217.6, Cr–C(Cp) and C–C(Cp) as for **6**. For **2**–**4**, **6**, and **7**: C–H(Cp) = 109, C–H(Me) = 96 pm.

Table 3. Parameters used in the extended Hückel calculations

Atom	Orbital	H_{ii} [eV][a]	ζ_1[b] (c_1[c])	ζ_2[b] (c_2[c])	Ref.
Cr	4s	−8.66	1.70		[43]
	4p	−5.24	1.70		
	3d	−11.22	4.95 (0.4876)	1.60 (0.7205)	
C	2s	−21.4	1.625		[23]
	2p	−11.4	1.625		
Cl	3s	−30.0	2.033		[44]
	3p	−15.0	2.033		
H	1s	−13.6	1.3		[23]

[a] Orbital energies. – [b] Slater exponents. – [c] Coefficients used in the double ζ expansion of the d orbitals.

This work was initially supported by the *Deutscher Akademischer Austauschdienst* through the award of a *NATO postdoctoral fellowship* to C. J. Current support by the *Deutsche Forschungsgemeinschaft*, the *Fonds der Chemischen Industrie* and the *Freunde der TU Berlin* is gratefully acknowledged by C. J. We thank *NATO* for a Collaborative Research grant (No. 86/0449) to J. S. and K. H. T., and the *National Science Foundation* for generous support through grant CHE-8820354 to K. H. T.

[1] F. A. Cotton, R. A. Walton, *Multiple Bonds Between Metal Atoms*, Wiley-Interscience: New York, **1982**; F. A. Cotton, R. A. Walton, *Struct. Bonding (Berlin)* **1985**, *62*, 1.
[2] F. A. Cotton, G. Wilkinson, in *Advanced Inorganic Chemistry*, Wiley-Interscience: New York, 5th ed., **1988**, chapter 23, p. 1052.
[3] R. D. Davy, M. B. Hall, *J. Am. Chem. Soc.* **1989**, *111*, 1268; and references therein.
[4] J. J. H. Edema, S. Gambarotta, *Comments Inorg. Chem.* **1991**, *11*, 195; J. J. H. Edema, S. Gambarotta, A. Meetsma, A. L. Spek, *Organometallics* **1992**, *11*, 2452; J. Losada, S. Alvarez, J. J. Novoa, F. Mota, R. Hoffmann, J. Silvestre, *J. Am. Chem. Soc.* **1990**, *112*, 8998.
[5] F. A. Cotton, G. Wilkinson, *Advanced Inorganic Chemistry*, Wiley-Interscience: New York, 5th ed., **1988**, p. 688; L. Spiccia, G. D. Fallon, A. Markiewicz, K. S. Murray, H. Riesen, *Inorg. Chem.* **1992**, *31*, 1066.
[6] S. S. Shaik, R. Hoffmann, C. R. Fisel, R. H. Summerville, *J. Am. Chem. Soc.* **1980**, *102*, 4555.
[7] D. S. Richeson, S.-W. Hsu, N. H. Fredd, G. Van Duyne, K. H. Theopold, *J. Am. Chem. Soc.* **1986**, *108*, 8273.
[8] S. K. Noh, S.C. Sendlinger, C. Janiak, K. H. Theopold, *J. Am. Chem. Soc.* **1989**, *111*, 9127.
[9] S. K. Noh, R. A. Heintz, C. Janiak, S. C. Sendlinger, K. H. Theopold, *Angew. Chem.* **1990**, *102*, 805; *Angew. Chem. Int. Ed. Engl.* **1990**, *29*, 775.
[10] S. K. Noh, R. A. Heintz, K. H. Theopold, manuscript in preparation.
[11] K. H. Theopold, *Acc. Chem. Res.* **1990**, *23*, 263; B. J. Thomas, S. K. Noh, G. K. Schulte, S. C. Sendlinger, K. H. Theopold, *J. Am. Chem. Soc.* **1991**, *113*, 893.
[12] R. L. Martin, in *New Pathways of Inorganic Chemistry* (Ebsworth, Maddock, Sharp, Eds.), Cambridge, University, **1968**; chapter 9; R. L. Carlin, *Magnetochemistry*, Springer, Berlin, **1968**; chapter 5.
[13] We point to a recent structure-magnetism correlation for face-sharing d^3-d^3 complexes: A. Niemann, U. Bossek, K. Wieghardt, C. Butzlaff, A. X. Trautwein, B. Nuber, *Angew. Chem.* **1992**, *104*, 345; *Angew. Chem. Int. Ed. Engl.* **1992**, *31*, 311.
[14] W. C. Hamilton, *Proc. Royal Soc. London* **1956**, *A235*, 395; E. A. Laws, R. M. Stevens, W. N. Lipscomb, *J. Am. Chem. Soc.* **1972**, *94*, 4461; R. McWeeny, in *Valence* (C. A. Coulson, Ed.), Oxford University Press: Oxford, **1979**, 3rd ed., p. 363.
[15] A. H. Cowley, W. D. White, *J. Am. Chem. Soc.* **1969**, *91*, 34; K. A. Levison, P. G. Perkins, *Theor. Chim. Acta* **1970**, *17*, 1; 15; M. E. O'Neill, K. Wade, in *Comprehensive Organometallic Chemistry* (G. Wilkinson, F. G. A. Stone, E. W. Abel, Eds.), Pergamon Press: Oxford, **1982**, vol. 1, p. 10; J. J. Eisch, *ibid.*, p. 582.
[16] B. F. G. Johnson, J. Lewis, P. A. Kilty, *J. Chem. Soc. (A)* **1968**, 2859; R. Mason, *Special Lectures XXIII IUPAC Congress*, **1971**, *6*, 31; R. Mason, D. M. P. Mingos, *J. Organomet. Chem.* **1973**, *50*, 53.
[17] **11**: G. Allegra, G. Perego, A. Immirzi, *Makromol. Chem.* **1963**, *61*, 69; **12**: V. R. Magnuson, G. D. Stucky, *J. Am. Chem. Soc.* **1969**, *91*, 2544; **13**: J. C. Huffman, W. E. Streib, *J. Chem. Soc. Chem. Commun.* **1971**, 911.
[18] Positive charge serves to remove the contribution from the d block frontier orbitals.
[19] F. A. Cotton, D. A. Ucko, *Inorg. Chim. Acta* **1972**, *6*, 161; and references therein.
[20] F. A. Cotton, *Pure Appl. Chem.* **1967**, *17*, 25.
[21] R. H. Summerville, R. Hoffmann, *J. Am. Chem. Soc.* **1979**, *101*, 3821.
[22] See also: R. Poli, H. D. Mui, *Inorg. Chem.* **1991**, *30*, 65.
[23] R. Hoffmann, *J. Chem. Phys.* **1963**, *39*, 1397; R. Hoffmann, W. N. Lipscomb, *ibid.* **1962**, *37*, 2872; **1962**, *36*, 2179.
[24] For various quantitative treatments of magnetic properties using ab-initio methods, see: L. Noodleman, B. J. Baerends, *J. Am. Chem. Soc.* **1984**, *106*, 2316; P. de Loth, P. Cassoux, J. P. Daudey, J. P. Malrieu, *ibid.* **1981**, *103*, 4007; M. M. Goodgame, W. W. Goddard III, *J. Phys. Chem.* **1981**, *85*, 215; *Phys. Rev. Lett.* **1982**, *48*, 135; Noodleman describes an approach to a description of antiferromagnetic coupling with the help of X-α calculations; in L. Noodleman, *J. Chem. Phys.* **1981**, *74*, 5735.
[25] Descriptions of magnetic properties from semi-quantitative calculations have been proposed in: P. J. Hay, J. C. Thibeault, R. Hoffmann, *J. Am. Chem. Soc.* **1975**, *97*, 4884; O. Kahn, B. Briat, *J. Chem. Soc., Faraday Trans. 2*, **1976**, *72*, 268; **1976**, *72*, 1441; O. Kahn, B. Briat, J. Gely, *J. Chem. Soc., Dalton Trans.* **1977**, 1453; O. Kahn, M. F. Charlot, *Nouv. J. Chim.* **1980**, *4*, 567; J. J. Girerd, Y. Journaux, O. Kahn, *Chem. Phys. Lett.* **1981**, *82*, 534; M. F. Charlot, O. Kahn, M. Chaillet, C. Larrieu, *J. Am. Chem. Soc.* **1986**, *108*, 2574; O. Kahn, *Angew.Chem.* **1985**, *97*, 837; *Angew. Chem. Int. Ed. Engl.* **1985**, *24*, 834.
[26] Yu. V. Rakitin, V. T. Kalinnikov, M. V. Eremin, *Theor. Chim. Acta* **1977**, *45*, 167; M. V. Eremin, Yu. V. Rakitin, *Phys. Stat. Sol.* **1977**, *80B*, 579.
[27] F. A. Cotton, J. L. Eglin, R. L. Luck, K. Son, *Inorg. Chem.* **1990**, *29*, 1802; F. H. Köhler, J. Lachmann, G. Müller, H. Zeh, H. Brunner, J. Pfauntsch, J. Wachter, *J. Organomet. Chem.* **1989**, *365*, C15.
[28] R. H. Summerville, R. Hoffmann, *J. Am. Chem. Soc.* **1976**, *98*, 7240.
[29] J. Silvestre, R. Hoffmann, *Inorg. Chem.* **1985**, *24*, 4108.
[30] Here, we mean spin-paired configurations. In reality the situation is much more complex since Slater determinants of overall S = 0 spin with unpaired α and β spins will also contribute to the singlet state.
[31] [31a] Y. Jiang, A. Tang, R. Hoffmann, J. Huang, J. Lu, *Organometallics* **1985**, *4*, 27; and references therein. – [31b] P. Hofmann, N. Rösch, H. R. Schmidt, *Inorg. Chem.* **1986**, *25*, 4470.
[32] S. C. Chang, G. A. Jeffrey, *Acta Crystallogr., Sect. B*, **1970**, *26*, 673; F. A. Cotton, W. Wang, *Inorg. Chem.* **1982**, *21*, 2675.
[33] L. B. Handy, J. K. Ruff, L. F. Dahl, *J. Am. Chem. Soc.* **1970**, *92*, 7312; H. Vahrenkamp, *Chem. Ber.* **1978**, *111*, 3472; J. L. Calderon, S. Fontana, E. Frauendorfer, V. W. Day, *J. Organomet. Chem.* **1974**, *64*, C10; A. T. McPhail, G. A. Sim, *J. Chem. Soc. A*, **1968**, 1858.
[34] We consider unlikely the possibility of *inter*molecular ferromagnetic coupling.
[35] T. A. Albright, J. K. Burdett, M. H. Whangbo, *Orbital Interactions in Chemistry*, Wiley-Interscience, New York, **1985**.
[36] F. A. Cotton, *Chemical Applications of Group Theory*, Wiley-Interscience, New York, **1971**, 2nd ed.
[37] An a_2 representation comes in for orbitals featuring a node in the mirror planes passing through the chromium and opposite chlorine atoms.

[38] A. Dedieu, T. A. Albright, R. Hoffmann, *J. Am. Chem. Soc.* **1979**, *101*, 3141.
[39] M. H. Whangbo, M. J. Foshee, R. Hoffmann, *Inorg. Chem.* **1980**, *19*, 1723.
[40] P. Dapporto, S. Midollini, L. Sacconi, *Inorg. Chem.* **1975**, *14*, 1643.
[41] R. Bau, W. E. Carroll, D. W. Hart, R. G. Teller, T. F. Koetzle, *Adv. Chem. Ser.* (Trans. Met. Hydrides) (R. Bau, Ed.) **1973**, *167*, 73.
[42] J. H. Ammeter, H.-B. Bürgi, J. C. Thibeault, R. Hoffmann, *J. Am. Chem. Soc.* **1978**, *100*, 3686.
[43] T. A. Albright, P. Hofmann, R. Hoffmann, C. P. Lillya, P. A. Dobosh, *J. Am. Chem. Soc.* **1983**, *105*, 3396.
[44] D. L. Thorn, R. Hoffmann, *J. Am. Chem. Soc.* **1978**, *100*, 2079; R. A. Wheeler, M. H.Whangbo, T. Hughbanks, R. Hoffmann, J. K. Burdett, T. A. Albright, *J. Am. Chem. Soc.* **1986**, *108*, 2222.

[345/92]